Respiratory Research

RESEARCH

Open Access

Harmine alleviates LPS-induced acute lung injury by inhibiting CSF3-mediated MAPK/NF-κB signaling pathway

Yihui Zhai[1], Kejie Chen[1], Zichuang Xu[1], Xiaojian Chen[1], Jiaying Tong[1], Yeying He[1], Chaoyue Chen[1], Meiqing Ding[1], Guang Liang[1*] and Xiaohui Zheng[1*]

Abstract

Background Acute lung injury (ALI) is a life-threatening inflammatory lung disease that lacks safe and effective treatment strategies. Harmine, an alkaloid derived from Peganum harmala L plants, exhibits anti-inflammatory activity. However, the protective effect of harmine against ALI and its underlying mechanism remain unknown. This study aimed to elucidate the therapeutic effects and molecular mechanisms of harmine against ALI.

Methods The therapeutic effects of harmine were assessed in LPS-induced ALI mice. Serum, bronchoalveolar lavage fluid (BALF), lung tissues were routinely analyzed to evaluated disease severity. The anti-inflammatory mechanism was elucidated in LPS-simulated RAW264.7 cells using a series assays, including RNA-seq, gene silencing, immunofluorescence, western blotting, co-immunoprecipitation and bioinformatic analysis. The biological safety of harmine was determined both in vitro and in vivo through cytotoxicity test, long-term cell proliferation test, acute toxicity test in mice, and assessments of liver and kidney function and structural changes.

Results The results showed that harmine inhibited the expression and secretion of LPS-induced inflammatory factors (IL-6, IL-1β and TNF-α) and reduced inflammatory cell infiltration in the lungs, resulting in alleviated LPS-induced histopathological changes and injury in mice. Mechanically, the findings revealed that harmine does not disrupt the TLR4-MD2 interaction but instead attenuates inflammation by suppressing CSF3 transcription and expression, leading to the inhibition of the MAPK/NF-κB signaling pathway activation induced by LPS stimulation. Additionally, both in vitro and in vivo studies demonstrated that harmine administration does not exhibit obvious cytotoxicity or long-term cell proliferation inhibition, nor does it cause functional or organic lesions the liver and kidney in mice, or other acute toxic effects.

Conclusions These findings elucidated that the anti-inflammatory activity of harmine was achieved through the CSF3-mediated inactivation of the MAPK/NF-κB signaling pathway, suggesting that harmine could serve as a promising therapeutic drug for ALI and other inflammatory diseases.

*Correspondence:
Guang Liang
wzmcliangguang@163.com
Xiaohui Zheng
zhengxh@wmu.edu.cn

Full list of author information is available at the end of the article

Keywords Acute lung injury, MAPK/NF-κB signaling pathway, Harmine, Inflammatory, Granulocyte Colony-Stimulating factor (CSF3)

Background

Acute lung injury (ALI) is a life-threatening inflammatory lung disease caused by damage to alveolar epithelial cells and capillary endothelial cells [1, 2]. Up to 50% of ALI patients with severe infection will develop acute respiratory distress syndrome (ARDS), resulting in a mortality rate of up to 46% even with standard treatment [3–5]. The pathogenesis of ALI is complex and systemic inflammation leads to serious complications, making clinical treatment challenging even in advanced medical settings [6]. Mechanical ventilation, fluid management and drug therapy based supportive treatments, remain the main clinical strategies for ALI [7]. However, these treatments often fail to meet clinical expectations due to drawbacks such as inducing pulmonary edema and barotrauma, immunosuppression, and drug resistance, even multiple drug resistance. Although some new treatments are available for ALI patients [2, 8], these newly developed strategies, such as extracorporeal membrane oxygenation (ECMO), are expensive and complicated to administer [9]. Consequently, supportive therapy is still generally adopted to relieve patients suffering from ALI, although has limited positive effect on survival. Therefore, development of new targets, potential therapeutic drugs, and treatment strategies for ALI is urgent.

MAPK and NF-κB signaling pathways, which interact synergistically to regulate the extent and duration of the inflammatory response, play a critical role in the inflammatory storm in ALI [10, 11]. Currently, anti-inflammatory treatment of ALI has achieved expected therapeutic effect mainly by regulating these pathways [12–14]. CSF3, also known as Granulocyte Colony-Stimulating Factor (G-CSF), is a cytokine that plays an important role in the regulation of inflammation and immune response [15–17]. It had been demonstrated that CSF3 regulates the MAPK and/or NF-κB signaling pathways [18–20]. For instance, CSF3 alleviated diabetes-induced cerebral vascular defects by activating the MAPK signaling pathway [21], improves depression-like behaviors by inhibiting the MAPK signaling pathways [22], and inhibits MAPK activities in CSF3-dependent neutrophil differentiation [23]. Additionally, CSF3 promotes neuronal cell autophagy by inhibiting the NF-κB signal pathway in an acute spinal cord injury mice model [24], and exhibits a positive correlation with NF-κB protein levels in the hippocampi of mice [25]. Overall, previous studies demonstrate a close regulatory association between CSF3 and the MAPK or NF-κB signaling pathways in non-inflammatory diseases. Moreover, CSF3 also act as a potential inflammatory mediator in BALF and serum [26], and can induce ALI in rats [27, 28]. Thus, CSF3 might be a valuable new target in ALI treatment, and although not yet reported, warrants further exploration.

Harmine (PubChem CID: 5280953, Fig. 1A), an alkaloid derived from the natural plant *Peganum harmala L*, possesses multiple pharmacological activities, including anti-inflammatory, antibacterial, antitumor effects [29–31]. Evidence shows that harmine can inhibit the M1 phenotype polarization of macrophage RAW 264.7 and reduce the inflammatory response by inhibiting the activation of the STAT1/3, NF-κB and MAPK signaling pathways [32]. Additionally, harmine increases the level of anti-inflammatory factors by facilitating the polarization of macrophages from the M1 to the M2 phenotype, which plays a key role in the late stage of inflammation and expresses inhibitory inflammatory factors [33]. Moreover, studies suggest that harmine alleviates LPS-induced acute kidney injury in mice by inhibiting the TLR4-NF-κB/NLRP3 inflammasome signaling pathway [34]. Collectively, previous studies suggest that harmine may have a potential therapeutic effect on ALI by modulating inflammatory processes. Therefore, to explore harmine as a potential therapeutic agent for ALI and further enrich its pharmacological profile, its therapeutic effect and underlying mechanism were investigated in an LPS-induced ALI mouse model and RAW 264.7 cells. The results indicate that harmine alleviates LPS-induced ALI in mice by inhibiting the MAPK/NF-κB pathway through suppressing the transcription and expression of CSF3.

Materials and methods

Reagents and antibodies

Harmine (Cat. No. 442-51-3) was sourced from TargetMol (Shanghai, China). LPS (Cat. No. 325D031) was obtained from Solarbio. Antibodies against β-Actin (Cat. No. 13E5), P38 (Cat. No. 9212 S), phosphorylated P38 (p-P38) (Cat. No. 9211 S), c-Jun N-terminal kinase (JNK; Cat. No. 9252 S), p-JNK (Cat. No. 4668 S), extracellular signal-regulated kinase (ERK; Cat. No. 4695 S), p-ERK (Cat. No. 4695 S), NF-κB P65 (Cat. No. D14E12), p-P65 (Cat. No. 3033 S), IκBα (Cat. No. 4812 S), p-IκBα (Cat. No. 2859 S), Lamin B1 (Cat. No. 13435 S), anti-rabbit IgG (No. 7074) and anti-mouse IgG (No. 7076) were from Cell Signaling Technology (Danvers, MA). Antibodies against TLR4

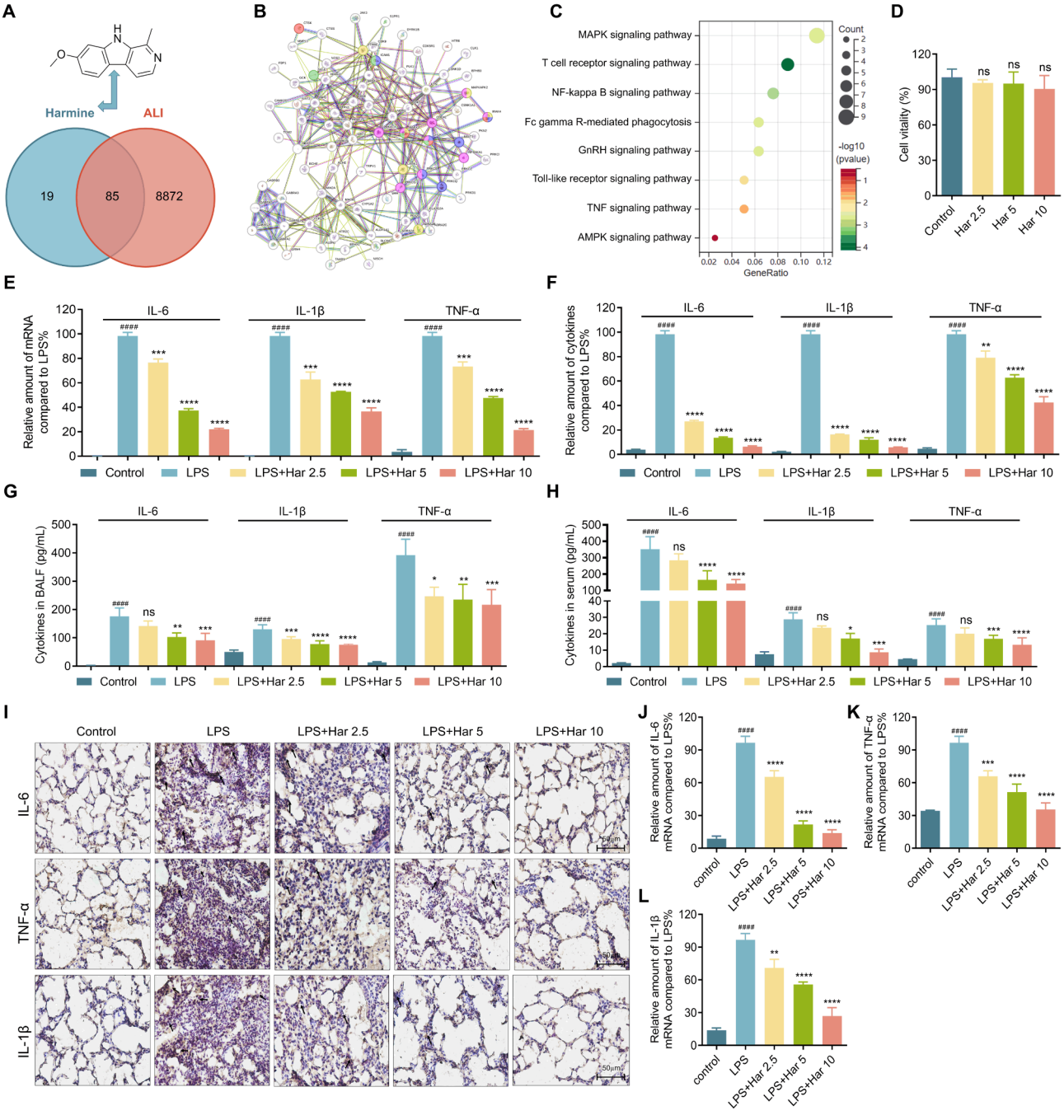

Fig. 1 Harmine inhibited LPS-induced inflammation. (**A**) Venn diagram of the cross target between the therapeutic target of harmine and ALI. (**B**) PPI network with 85 overlapping targets, colored circular nodes represent inflammation related targets. (**C**) KEGG enrichment analysis of the 85 overlapping genes. (**D**) The cell viability of harmine against RAW264.7 cells at the indicated dose. (**E**) qPCR assay determined the IL-6, IL-1β and TNF-α mRNA levels in RAW264.7 cells. Before used, cells were pretreated with the indicated dose of harmine for 30 min, followed by exposing to LPS (0.5 μg/mL) for 6 h. (**F**) ELISA assay determined the secretion of IL-6, IL-1β and TNF-α protein. The cells were treated the same as (E), except LPS stimulated for 12 h. (**G** and **H**) ELISA assay determined the cytokine content in BALF and serum of LPS-induced ALI mice. (**I**) Representative images of immunohistochemical staining in lung tissue. Scale bar, 50 μm. (**J**-**L**) The transcription of IL-6, IL-1β and TNF-α in lung were determined by qPCR. The LPS-induced ALI mouse model was established by administering LPS (5 mg/kg intratracheally) to C57BL/6 mice ($n=6$) with or without pretreated with harmine at the indicated dose. Lung tissues, BALF and serum were collected 6 h after modeling. Values represent the mean ± SD of at least three independent experiments. ns, no significance; *$p<0.05$; **$p<0.01$; ***$p<0.001$, ****$p<0.0001$, vs. LPS group. $^{\#\#\#\#}p<0.0001$, vs. control group

(Cat. No. sc-293072), MD2 (Cat. No. sc-80183), macrophage markers Ly-6G (Cat. No. sc-53515) and F4/80 (Cat. No. sc-377009) were purchased from Santa Cruz Biotechnology (Dallas, TX). The IL-6 antibody (Cat. No. 26404-1-AP), TNF-α (Cat. No. 26405-1-AP) and IL-1β (Cat. No. 26048-1-AP) were obtained from Proteintech (Wuhan, China). Mouse TNF-α ELISA Kit (88-7324-86), Mouse IL-1β ELISA Kit (88–7013 A-88) and Mouse IL-6 ELISA Kit (88-7064-86) were procured from Thermo Fisher Scientific (USA). The DyLight 488-conjugated anti-Rabbit (No. SA00013-2), for immunofluorescence assays, was purchased from Proteintech (Wuhan, China). BeyoClick™ EdU Cell Proliferation Kit with Alexa Fluor 555 (No. C0075L) was obtained from Beyotime (Shanghai, China). The Annexin V-FITC Apoptosis Assay Kit (No. 556547) was purchased from BD Biosciences (USA). Alanine aminotransferase (ALT) Assay Kit (C009-2-1), Aspartate aminotransferase (AST) Assay Kit (C010-1-1), and Creatinine (Cr) Assay kit (C011-2-1) were purchased from Nanjing Jiancheng Bioengineering Institute (Nanjing, China).

Drug administration

In the in vitro experiments, harmine was initially prepared as a 10 mM solution in DMSO and then diluted to the indicated concentrations using DMEM or MEM. The control group received a medium containing 0.1% DMSO. In the in vivo experiments, harmine was directly dissolved in a mixed solvent composed of anhydrous ethanol, TWEEN 80, and saline in a ratio of 1:1:6. The control group was administered an equal volume of the mixed solvent.

Animals and cells

Male C57BL/6 mice (18–22 g, 6–8 weeks old) were obtained from Charles River Laboratories (Beijing, China). All animal studies and experimental procedures were approved by Wenzhou Medical University Animal Policy and Welfare Committee (Approval Document No. xmsq2021-0043) in accordance with the National Institutes of Health (USA) guidelines.

RAW264.7 macrophage cells were obtained from the China Center for Type Culture Collection (Wuhan, China). Human normal lung cell lines (BEAS-2B and MRC-5) were purchased from the Institute of Biochemistry and Cell Biology, Chinese Academy of Sciences (China). BEAS-2B and RAW264.7 cells were cultured in DMEM (Gibco, USA), MRC-5 cells were cultured in MEM (Gibco, USA), and all cells were maintained at 37 °C with 5% CO_2. The media for all cells was supplemented with 10% fetal calf serum (Gibco, USA), 100 U/mL penicillin and streptomycin (Hyclone, Logan, UT).

Construction of acute lung injury mouse model

The mice were acclimated for a week and provided with ad libitum access to food and water. Mice were randomly assigned to five groups, ($n = 6$ per group): control group (Control), ALI group (LPS, intratracheal instillation of LPS at 5 mg/kg), ALI + harmine treatment groups (LPS + harmine: LPS + Har 2.5 mg/kg, LPS + Har 5 mg/kg, and LPS + Har 10 mg/kg). For preventive study: the mice in each group were administered harmine or mixed solvent via intraperitoneal injection (*i.p.*) 24, 12 and 1 h before modeling. For therapeutic study: mice were intraperitoneally injected with harmine (2.5 mg/kg, 5 mg/kg or 10 mg/kg) one hour after intratracheal instillation of 5 mg/kg LPS. 6 h after intratracheal infusion of LPS stimulation, the mice were sacrificed, then serum, bronchoalveolar lavage fluid (BALF), and tissue samples were collected and stored at -80 ℃ for future use.

Cell viability assay

The cell viability assay was conducted following previously described methods [35]. Additional details are provided in the Supplementary Information.

Colony formation assay

The colony formation assay was conducted following previously described methods [35]. Additional details are provided in the Supplementary Information.

EdU staining assay

The EdU staining assay was conducted following previously described methods [36]. Additional details are provided in the Supplementary Information.

Annexin V/PI apoptosis assay

The Annexin V/PI apoptosis assay was conducted following previously described methods [35]. Additional details are provided in the Supplementary Information.

Lung wet/dry ratio

Lung wet/dry ratio was determined following previously described methods [37]. Additional details are provided in the Supplementary Information.

BALF analysis

BALF analysis was determined following previously described methods [37]. Additional details are provided in the Supplementary Information.

Hematoxylin-eosin (H&E) and immunohistochemical (IHC) staining

H&E and IHC staining assays were conducted following previously described methods [38]. Additional details are provided in the Supplementary Information.

Lung pathological score

Lung impairment was evaluated using a lung injury score ranging from 0 (normal) to 3 (severe) in four categories [39]: inflammatory cell infiltration, alveolar hemorrhage, alveolar edema, pulmonary interstitial edema. The lung pathological changes were assessed in a blinded manner, and the lung injury score was calculated by the sum of these four aspects.

ELISA determination of cytokines

The levels of IL-6, IL-1β and TNF-α in cells, serum, and BALF were measured using enzyme-linked immunosorbent assay (ELISA) kits. Specifically, the Mouse TNF-α ELISA Kit (88-7324-86, Invitrogen, USA), Mouse IL-1β ELISA Kit (88–7013 A-88, Invitrogen, USA), and Mouse IL-6 ELISA Kit (88-7064-86, Invitrogen, USA) were utilized according to the manufacturer's instructions.

Real-time quantitative PCR

Real-time quantitative PCR assay was described previously [37]. Details can be found in the Supplementary information. The sequence of primers is shown in Table S1.

RNA library construction and sequencing assay

Cells were pretreated with 10 μM harmine for 30 min, followed by exposure to LPS (0.5 μg/mL) for 6 h. Total RNA was extracted using TRIzol reagent (Thermo Fisher), and paired-end sequencing was conducted on an Illumina HiSeq 4000 at LC-BIO Technologies (Hangzhou), following the vendor's recommended protocol.

Transfection analysis

Transfection studies were conducted following previously described methods [36]. Additional details are provided in the Supplementary Information. The sequence of small interfering RNA is shown in Table S2.

Western blot assay

The western blot assay was conducted following previously described methods [35]. Additional details are provided in the Supplementary Information.

Immunofluorescence (IF) assay

The IF assay was conducted following previously described methods [35]. Additional details are provided in the Supplementary Information.

Co-immunoprecipitation (Co-IP) assay

The Co-IP assay was conducted following previously described methods [37]. Additional details are provided in the Supplementary Information.

Toxicity evaluation of harmine in vivo

C57BL/6J mice were randomly divided into 4 groups ($n = 6$ per group): control group (Control) and harmine (10, 30, 90 mg/kg) group. After different concentrations of harmine and mixed solvent were orally separately, the body weight was recorded daily for 7 days. On day 7, blood samples were collected. The heart, kidney, liver, and lung tissues were collected and weighed. Levels of serum alanine transaminase (ALT), aspartate aminotransferase (AST) and creatinine (Cr) activities were measured by kit. The pathological damage of each tissue was demonstrated by H&E staining.

Protein targets prediction of Harmine against ALI

The 2D chemical structure of harmine (CID:5280953) was downloaded from the PubChem public database (https://pubchem.ncbi.nlm.nih.gov/), and submitted to the PharmMapper database, with the target protein species parameter set to human and all other parameters left as default. Potential protein targets were reverse-predicted based on structural similarity principle. Concurrently, harmine's SMILE expression was submitted to the SwissTarget Prediction dataset, also with species set to human and other parameters as default. By intersecting the predicted targets from both databases, 104 candidate protein targets were identified for further analysis. Additionally, 8,957 ALI disease targets were retrieved from GeneCards, OMIM, and the Therapeutic Target Database (TTD). Finally, by intersecting the 104 harmine targets with the 8,957 ALI genes, 85 candidate protein targets were identified.

Potential targets protein-protein interaction (PPI) and pathway enrichment analysis

A protein-protein interaction (PPI) network was constructed using the STRING database. The KEGG pathway analysis of candidate proteins followed a structured process: first, the candidate targets were submitted to the Database for Annotation, Visualization, and Integrated Discovery (DAVID) with species set to human. Next, KEGG-pathway, GOTERM_BP_DIRECT(BP), GOTERM_CC_DIRECT(CC), and GOTERM_MF_DIRECT(MF) categories were selected for Gene Ontology (GO) and KEGG enrichment analysis of the overlapping genes. The resulting pathways were used to generate GO histograms and KEGG enrichment bubble charts via http://www.bioinformatics.com.cn/.

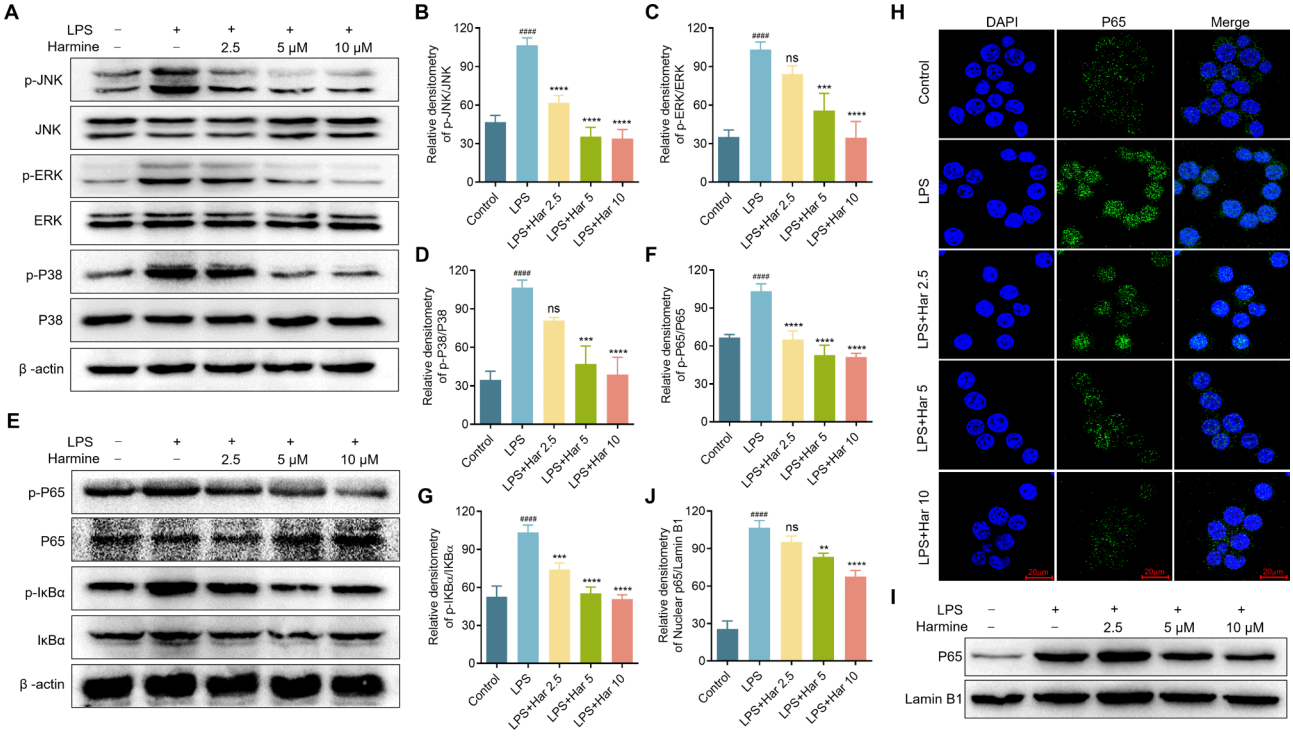

Fig. 2 Harmine inhibited LPS-induced MAPK and NF-κB signaling pathway activation in RAW264.7 cells. (**A** and **E**) The abundance of p-JNK, JNK, p-ERK, ERK, p-P38, P38, p-IκBα, IκBα, p-P65 and P65 proteins were measured using a western blot assay with β-actin serving as the loading control ($n = 3$). (**B**-**D** and **F**-**G**) Quantitative analyses of (**A**) and (**E**), respectively. (**H**) The translocation of P65 from the cytoplasm to the nucleus was examined using IF staining assay. Scale bar, 20 μm. (**I**) The NF-κB P65 subunit in the nucleus was measured by western blot assay, with Lamin B1 used as the loading control ($n = 3$). (**J**) Quantitative analysis of (**I**). Values represent as the mean ± SD of at least three independent experiments. ns, no significance; $^{**}p < 0.01$; $^{***}p < 0.001$, $^{****}p < 0.0001$, vs. LPS group. $^{\#\#\#\#}p < 0.0001$, vs. control group

Statistical analysis

All data were analyzed using GraphPad Prism 9.5. A two-tailed unpaired Student's t-test or one-way ANOVA was used to compare the means of two or more groups. All values are expressed as the mean ± standard deviation (SD) of at least three independent experiments. A significance level of $p < 0.05$ was defined as statistically significant.

Results

Harmine suppresses LPS-induced inflammation in a dose-dependent manner

To evaluate the potential preventive and therapeutic effect of harmine on ALI, 104 protein targets were identified using the SwissTarget database by incorporating harmine's chemical information from the PubChem database. The results indicated that these 104 potential targets overlapped with 85 of the 8957 ALI disease genes (Fig. 1A). A protein-protein interaction (PPI) network, constructed using the STRING database, revealed that these 85 overlapping targets are primarily involved in inflammation and its-related signaling pathways (Fig. 1B). Consistently, KEGG pathway enrichment analysis showed that the 85 overlapping target proteins are closely associated with the MAPK/NF-KB signaling pathway (Fig. 1C). These findings from network pharmacology indicated that harmine might exert a protective effect against ALI by inhibiting inflammatory responses.

First, the MTT assay was used to determine the non-toxic dose of harmine in RAW264.7 cells, both with and without LPS exposure (Fig. 1D and S1). Subsequently, LPS-stimulated RAW264.7 cells were treated with harmine at this non-cytotoxic dose to evaluate its anti-inflammatory activity. The results indicated that, compared to the control group, LPS stimulation significantly increased the transcription and secretion of IL-6, IL-1β and TNF-α in a dose-dependent manner (Fig. 1E-F). Similarly, harmine pretreatment showed comparable trends in BALF, serum, and lung tissues of LPS-induced ALI mice. Data from qPCR and ELISA assays demonstrated that harmine significantly decreased LPS-induced IL-6, IL-1β, and TNF-α protein levels in both BALF and serum (Fig. 1G-H). IHC staining indicated that LPS stimulation increased IL-6, IL-1β, and TNF-α immunoreactivity, but harmine pretreatment significantly reduced this increase (Fig. 1I), suggesting harmine inhibited LPS-induced recruitment of infiltrating cells. Consistent with this, qPCR analysis showed that the LPS-increased mRNA levels

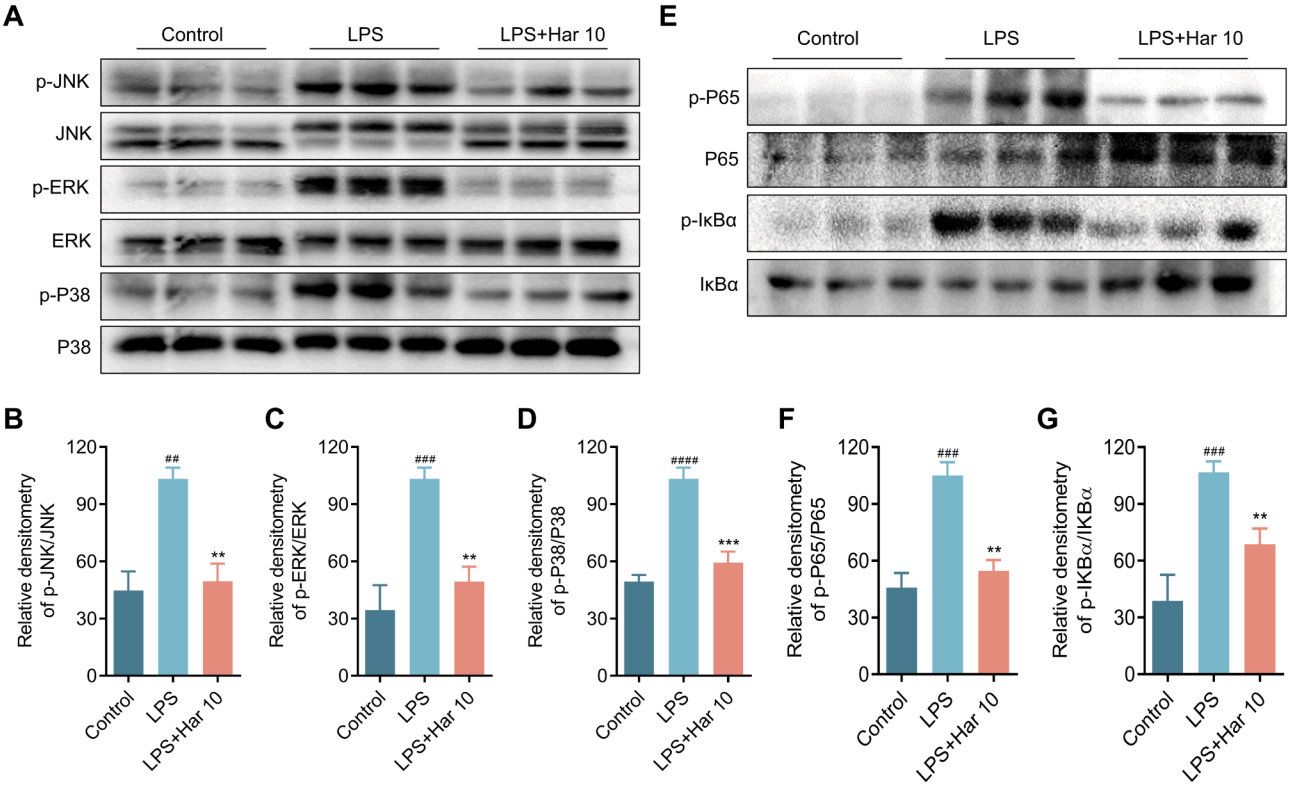

Fig. 3 Harmine inhibited the activation of MAPK and NF-κB signaling pathways in LPS-induced ALI mice. (**A** and **E**) The levels of p-JNK, JNK, p-ERK, ERK, p-P38, P38, p-IκBα, IκBα, p-P65 and P65 proteins were measured using a western blot assay ($n=3$). (**B**-**D** and **F**-**G**) Quantification of (**A**) and (**E**), respectively. The LPS-induced ALI mouse model was established by administering LPS (5 mg/kg intratracheally) to C57BL/6 mice ($n=6$) with or without pretreated with Harmine at the indicated dose. Lung tissues were collected 6 h after modeling. Values represent the mean ± SD of at least three independent experiments. $^{**}p<0.01$; $^{***}p<0.001$, vs. LPS group. $^{\#\#}p<0.01$; $^{\#\#\#}p<0.001$, $^{\#\#\#\#}p<0.0001$, vs. control group

of IL-6, IL-1β, and TNF-α in lung tissues were reduced by pretreatment with harmine (Fig. 1J-L). These findings showed that harmine significantly alleviates LPS-induced inflammation both in vitro and in vivo.

Harmine inhibits LPS-induced MAPK/NF-κB signaling pathway activation

Further investigation was conducted to evaluate the effects of harmine on LPS-induced inflammatory response downstream signaling, specifically MAPKs and NF-κB activation. The results showed that harmine reversed the elevated levels of ERK, JNK, and P38 phosphorylation induced by LPS stimulation in RAW264.7 cells (Fig. 2A), demonstrating that harmine inhibited LPS-induced MAPK signaling pathway activation. Quantitative analysis indicated that harmine decreased the abundance of p-ERK, p-JNK, and p-P38 in a dose-dependent manner (Fig. 2B-D). Additionally, the LPS-activated NF-κB signaling pathway, illustrated by increased p-P65 and p-IκBα protein levels, was markedly reduced by harmine pretreatment (Fig. 2E-G). Moreover, IF staining showed that LPS stimulation promoted the translocation of P65 from the cytoplasm to the nucleus in RAW264.7 cells, which was blocked by harmine in a dose-dependent manner (Fig. 2H). Consistent with the IF assay, the western blot assay indicated that harmine pretreatment significantly inhibited the LPS-induced increase of the NF-κB P65 subunit in the nucleus in a dose-dependent manner (Fig. 2I-J).

Similarly, compared to the control group, LPS-induced ALI lung tissues exhibited increased levels of p-ERK, p-JNK, and p-P38, while harmine pretreatment reduced the LPS-induced phosphorylation of these MAPKs (Fig. 3A-D). Additionally, lung tissues from LPS-induced ALI mice showed high expression of both p-P65 and p-IκBα, whereas in harmine pretreated ALI mice, the levels of p-P65 and p-IκBα were effectively reduced (Fig. 3E-G). Taken together, these results suggested that harmine reduces LPS-induced inflammatory response by inhibiting the MAPK/NF-κB signaling pathway.

Harmine alleviates LPS-induced ALI in mice through reduced infiltration

These findings promoted us to evaluate the preventive and therapeutic effect of harmine against LPS-induced ALI. The results showed that, compared to the control

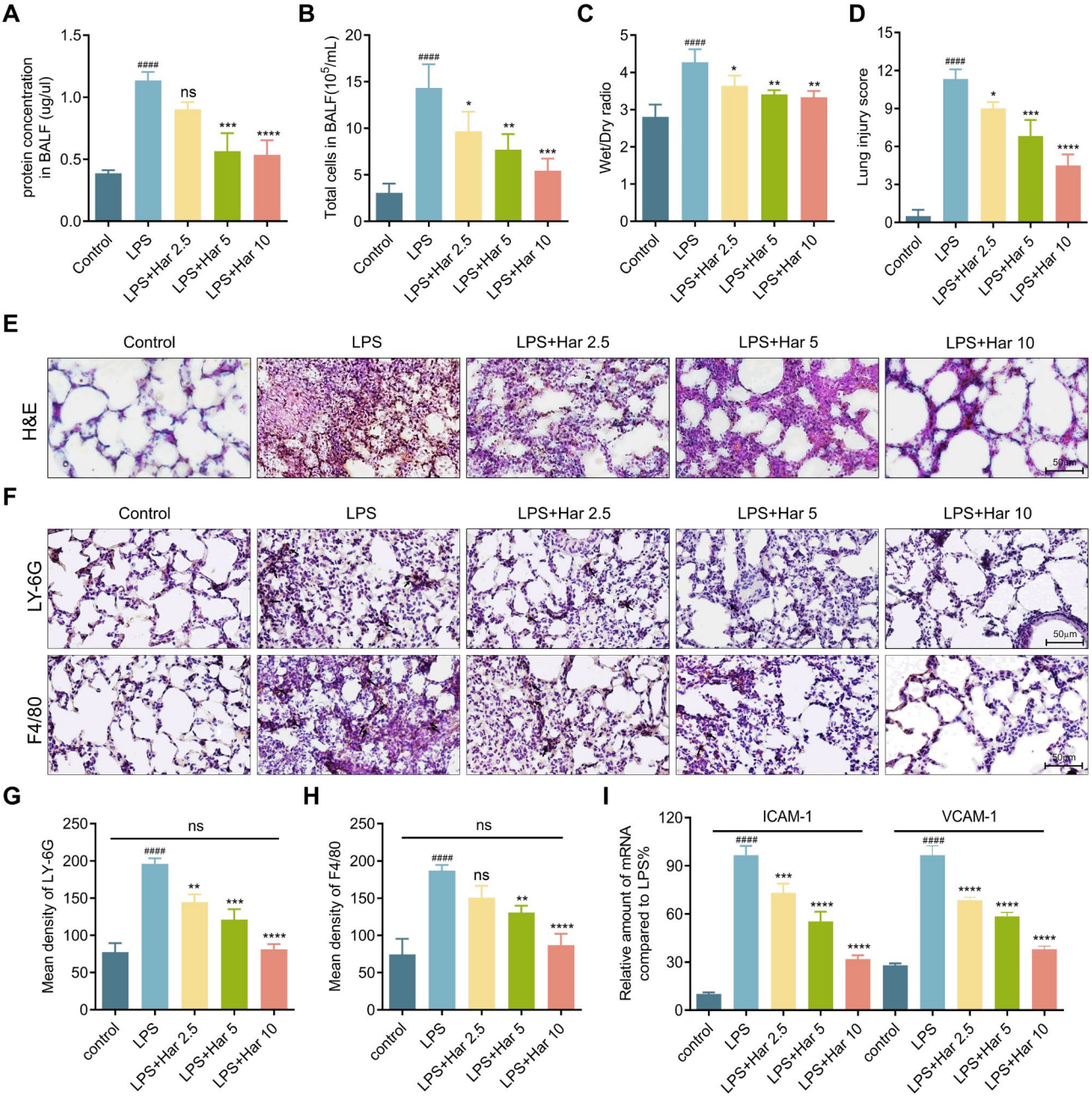

Fig. 4 Harmine pretreatment provided a protective effect on LPS-induced ALI mice. The LPS-induced ALI mouse model was established by administering LPS (5 mg/kg intratracheally) to C57BL/6 mice ($n = 6$) with or without pretreated with harmine at the indicated dose. BALF and lung tissues were collected 6 h after modeling and evaluated as follows. (**A**) Protein concentration of BALF supernatant. (**B**) Total cell counts in BALF. (**C**) Wet-dry weight ratio of lung tissue. (**D**) Lung injury score. (**E**) Representative images of H&E staining of lung tissue. Scale bar, 50 μm. (**F**) Representative images of IHC staining using LY-6G and F4/80 in lung tissue. Scale bar, 50 μm. (**G** and **H**) Quantitative analysis of (**F**). (**I**) ICAM-1 and VCAM-1 transcription levels in ALI lung tissue were determined by qPCR. Values represent the mean ± SD of at least three independent experiments. ns, no significance; $^{*}p < 0.05$; $^{**}p < 0.01$; $^{***}p < 0.001$, $^{****}p < 0.0001$, vs. LPS group. $^{\#\#\#\#}p < 0.0001$, vs. control group

group, LPS stimulation significantly increased the protein concentration and cell number in the BALF, along with the dry-wet weight ratio and lung injury score (Fig. 4A-D). However, harmine pretreatment reduced these increases (Fig. 4A-D). Histological analysis showed that LPS stimulation thickened the alveolar walls and increased infiltration of inflammatory cells and blood cells (Fig. 4E). Harmine reversed these LPS-induced histological changes, suggesting it alleviated LPS-induced ALI in mice (Fig. 4E). Moreover, the protective effect of harmine on LPS-induced ALI

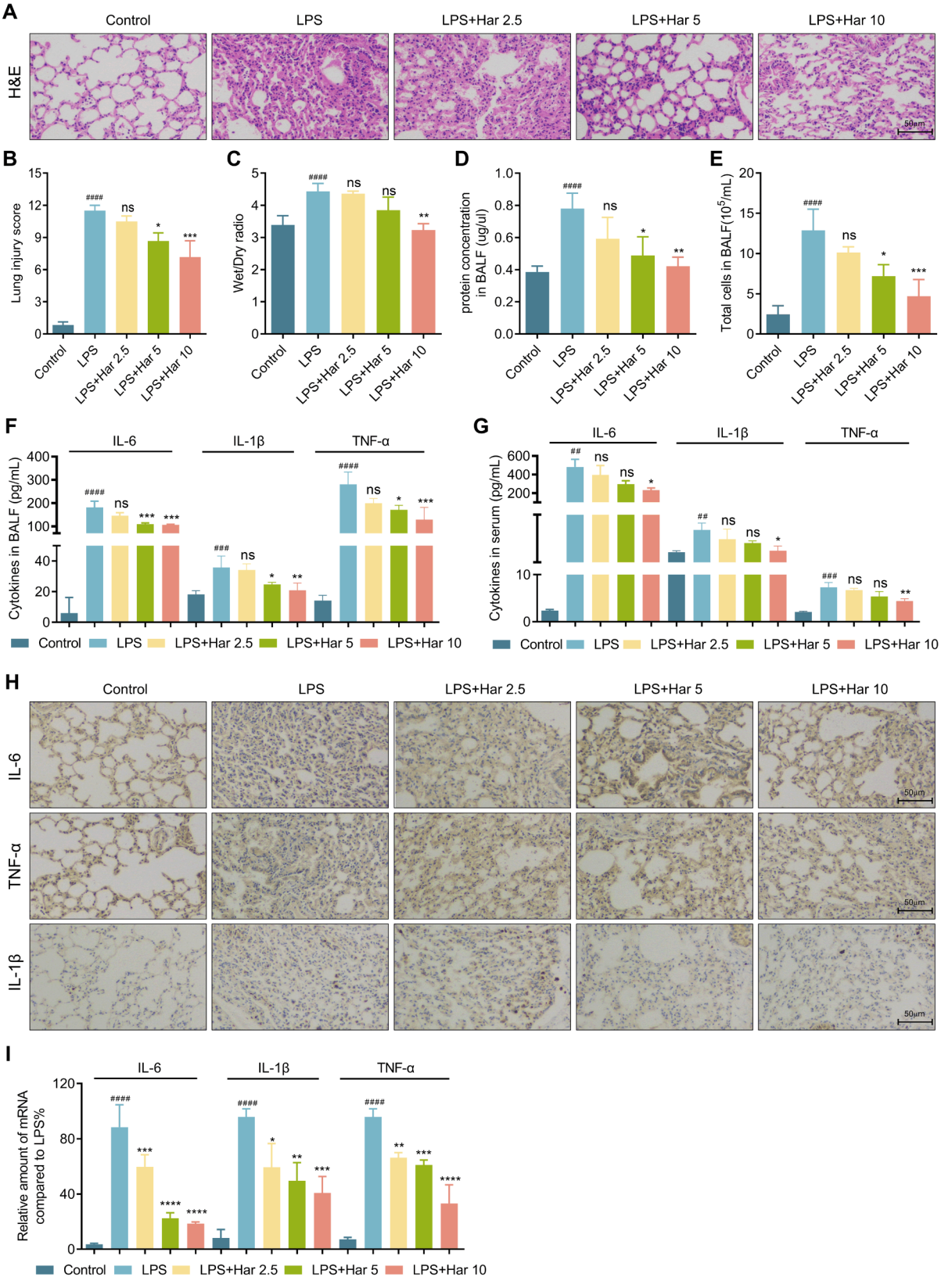

Fig. 5 (See legend on next page.)

(See figure on previous page.)

Fig. 5 Harmine showed therapeutic effects in mice with LPS-induced ALI. C57BL/6 mice were intraperitoneally injected harmine at the indicated dose (2.5 mg/kg, 5 mg/kg or 10 mg/kg) 1 h after intratracheal injection of 5 mg/kg LPS. Lung tissues, BALF and serum were collected 6 h after LPS injection. (**A**) Representative H&E staining images of the lung. (**B**) Lung injury score as assessed by histological analysis of lung tissues. (**C**) The lung wet/dry weight ratio. (**D**) Total proteins in BALF. (**E**) Total cells in BALF. The levels of IL-6, IL-1β and TNF-α in BALF (**F**) and serum (**G**) from the experimental mice were determined with ELISA. (**H**) Representative images of immunohistochemical staining in lung tissue. Scale bar, 50 μm. (**I**) The transcription of IL-6, IL-1β and TNF-α in lung were determined by qPCR. Values represent the mean ± SD of at least three independent experiments. ns, no significance; *$p < 0.05$; **$p < 0.01$; ***$p < 0.001$, ****$p < 0.0001$, vs. LPS group. $^{\#\#\#\#}p < 0.0001$, vs. control group

was dose-dependent, with the most pronounced effect observed at a dose of 10 mg/kg dose (Fig. 4E).

The abundance of inflammatory cytokines, primarily secreted by neutrophils and macrophages, is a key clinical indicator of ALI severity [40]. Therefore, the infiltration of neutrophils and macrophages was determined by IHC staining using LY-6G and F4/80 antibody, respectively (Fig. 4F). The statistical data showed that, compared to the control group, LPS stimulation significantly increased neutrophil and macrophage infiltration in lung tissues (Fig. 4G-H). However, harmine pretreatment significantly reduced the infiltration of these inflammatory cells, almost returning to control levels at 10 mg/kg (Fig. 4G-H). In addition to neutrophils and macrophages, intercellular adhesion molecule 1 (ICAM-1) and vascular cell adhesion molecule 1 (VCAM-1) play a crucial role in the inflammatory response of ALI [41]. As expected, qPCR results showed that both ICAM-1 and VCAM-1 mRNA transcription levels significantly elevated in LPS-induced

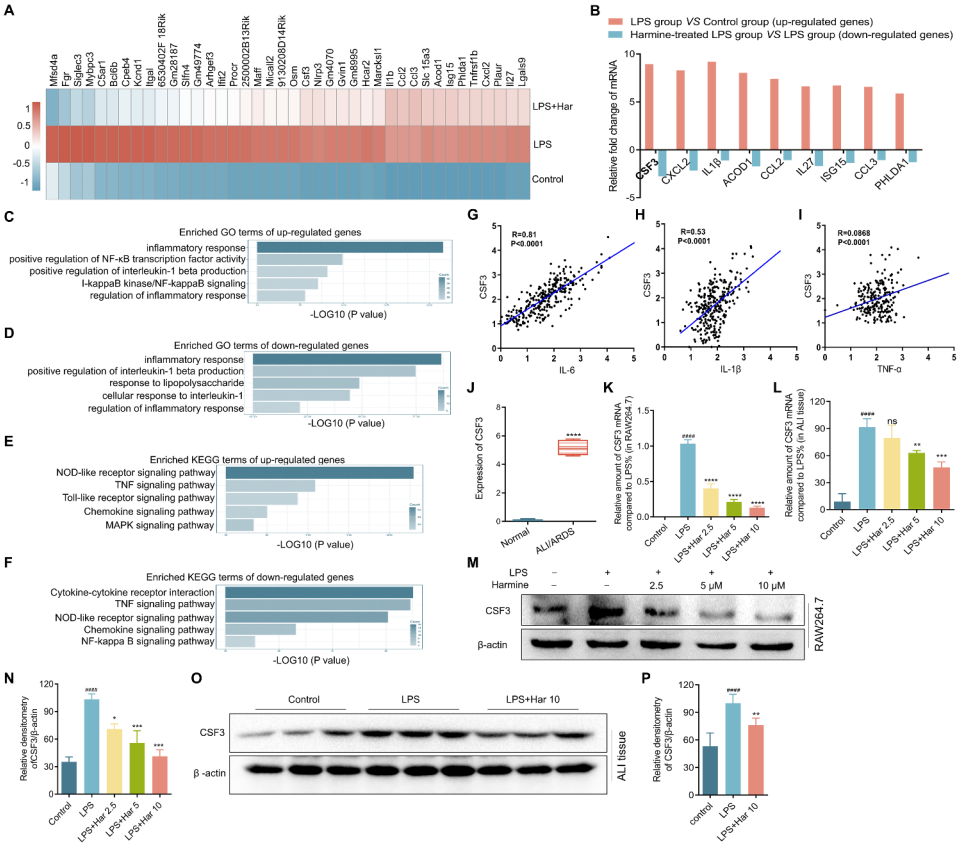

Fig. 6 Harmine inhibited the transcription and expression of CSF3 in LPS-stimulated RAW264.7 cells and lung tissue of LPS-induced ALI mice. Cells were pre-treated with 10 μM harmine for 30 min, followed by exposure to LPS (0.5 μg/mL) for 6 h before being used in RNA-seq, qPCR and western blot assays. C57BL/6 mice were pretreated with 10 mg/kg harmine via intraperitoneal injection (*i.p.*) 24, 12 and 1 h before intratracheal instillation 5 mg/kg LPS, and lung samples were obtained 6 h later. (**A**) Heat maps of the top 40 up-regulated genes induced by LPS stimulation and down-regulated genes in harmine-pretreated, LPS-stimulated RAW264.7 cells. (**B**) The top 10 most differentially up-regulated and down-regulated genes as in (**A**). (**C**-**F**) GO and KEGG enrichment analysis of up-regulated and down-regulated genes. (**G**-**I**) Bivariate analysis showing that CSF3 was positively correlated with IL-6, IL-1B and TNF-α. (**J**) GEO database analysis demonstrated that CSF3 was overexpressed in ALI/ARDS. (**K** and **L**) qPCR assay determined the CSF3 transcription levels in RAW264.7 cells and lung tissue, respectively. (**M** and **O**) Protein levels of CSF3 in RAW264.7 cells and lung tissue measured by western blot, respectively. β-actin as the loading control ($n = 3$). (**N** and **P**) Quantitative analysis of (M) and (O), respectively. Values represent as the mean ± SD of at least three independent experiments. *$p < 0.05$; ***$p < 0.001$, ****$p < 0.0001$, vs. LPS group. $^{\#\#\#\#}p < 0.0001$, vs. control group

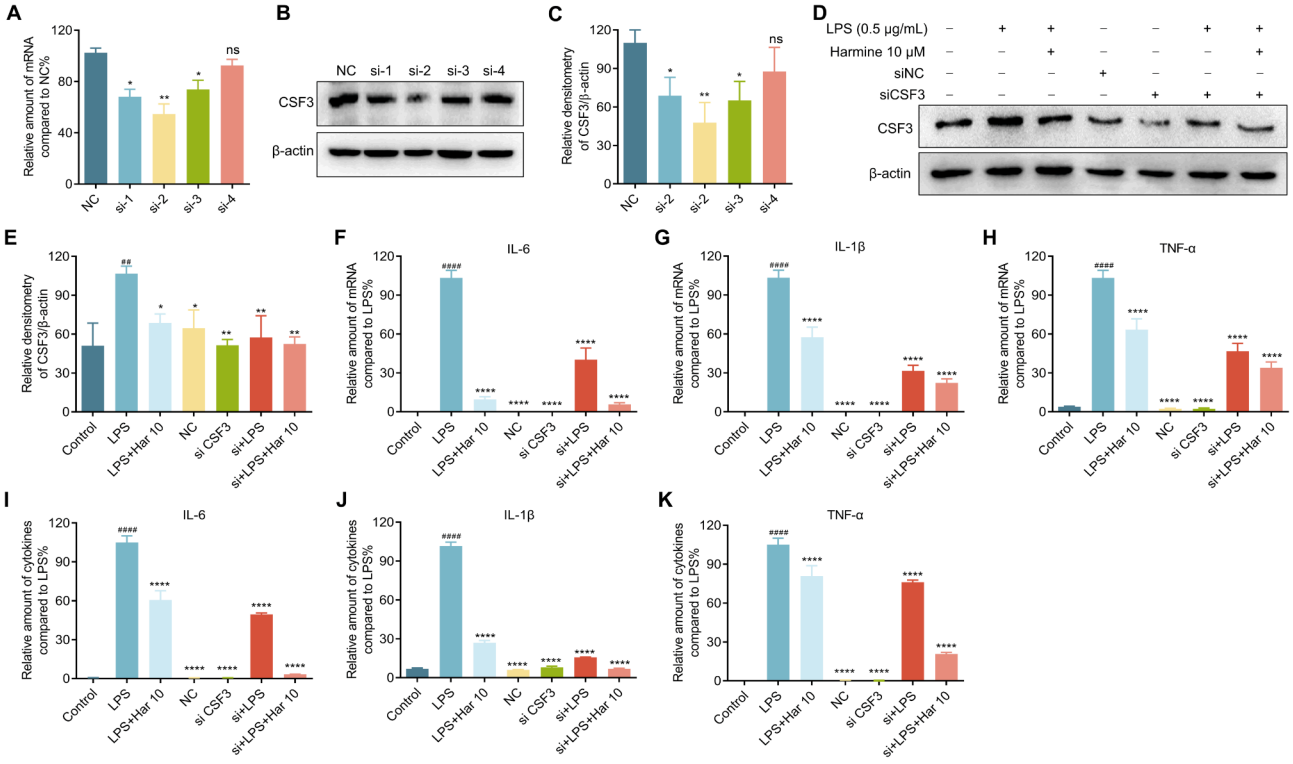

Fig. 7 Harmine inhibited CSF3-mediated inflammation in LPS-induced RAW264.7 cells. Cells was transfected with siRNA for 8 h, then pre-treated with harmine for 30 min, followed by exposure to LPS (0.5 μg/mL) for 6 h before being used in the following assays. (**A**) qPCR examined the transcript inhibitory efficacy of four candidate siRNAs. (**B**) Western blot determined the expression inhibitory efficacy of four candidate siRNAs ($n = 3$). (**C**) Quantitative analysis of (**B**). (**D**) The expression level of CSF3 protein was detected by western blot ($n = 3$). (**E**) Quantitative analysis of (**D**). (**F**-**H**) qPCR determined the IL-6, IL-1β and TNF-α mRNA transcription levels. (**I**-**K**) ELISA determined the expression levels of IL-6, IL-1β and TNF-α proteins in the supernatant. Values represent as the mean ± SD of at least three independent experiments. ns, no significance; *$p < 0.05$; **$p < 0.01$; ****$p < 0.0001$, vs. LPS group. $^{\#\#}p < 0.01$; $^{\#\#\#\#}p < 0.0001$, vs. control group

ALI lung tissues compared to the control group (Fig. 4I), and these levels were reduced under harmine pretreatment (Fig. 4I). These results confirmed that harmine significantly alleviates LPS-induced ALI in mice by inhibiting inflammatory cell infiltration.

Typically, drugs should be administered after lung injury onset. We evaluated the therapeutic effects of harmine in mice with LPS-induced ALI. Similar to the pretreatment experiment, our data demonstrated that harmine significantly reduced LPS-induced pathological injury of lung tissue (Fig. 5A-B), pulmonary edema (Fig. 5C), inflammatory cells infiltration in BALF (Fig. 5D-E), and elevated inflammatory cytokines IL-6, IL-1β and TNF-α levels in BALF, serum and lung tissue (Fig. 5F-I and S2). These findings indicated that harmine is effective for both prevention and therapy of LPS-induced ALI in mice.

Harmine exerts protective effect against LPS-induced ALI by inhibiting CSF3 transcription

As the TLR4-MD2 signaling pathway plays a crucial role in LPS-induced MAPK/NF-κB signaling pathway activation [37], the interaction of harmine with the TLR4-MD2 complex was assessed in LPS-stimulated RAW264.7 cells by Co-IP assays. We immunoprecipitated TLR4 and found no change in the levels of associated MD2 proteins when cells were pretreated with harmine before LPS stimulation (Fig. S3). These data indicated that harmine did not affect the interaction between TLR4 and MD2 as well as their expression. To elucidate the molecular mechanisms by which harmine inhibits the LPS-activated MAPK/NF-κB signaling pathway, RNA-seq analysis was conducted on 10 μM harmine-pretreated and untreated LPS-induced RAW264.7 cells. The full sequence data have been uploaded to the Gene Expression Omnibus (GEO) database under accession number GSE267507. Among the control, LPS-stimulation, and harmine pretreatment groups, the top 40 differentially expressed mRNAs and their abundances are presented in Fig. 6A. Among these genes, CSF3 was on the most significantly hit (Fig. 6B). Both GO and KEGG analyses suggested that these differentially expressed genes were mainly enriched in the MAPK/NF-κB signaling pathway (Fig. 6C-F). Additionally, bivariate analysis showed that CSF3 positively correlated with IL-6, IL-1β, and

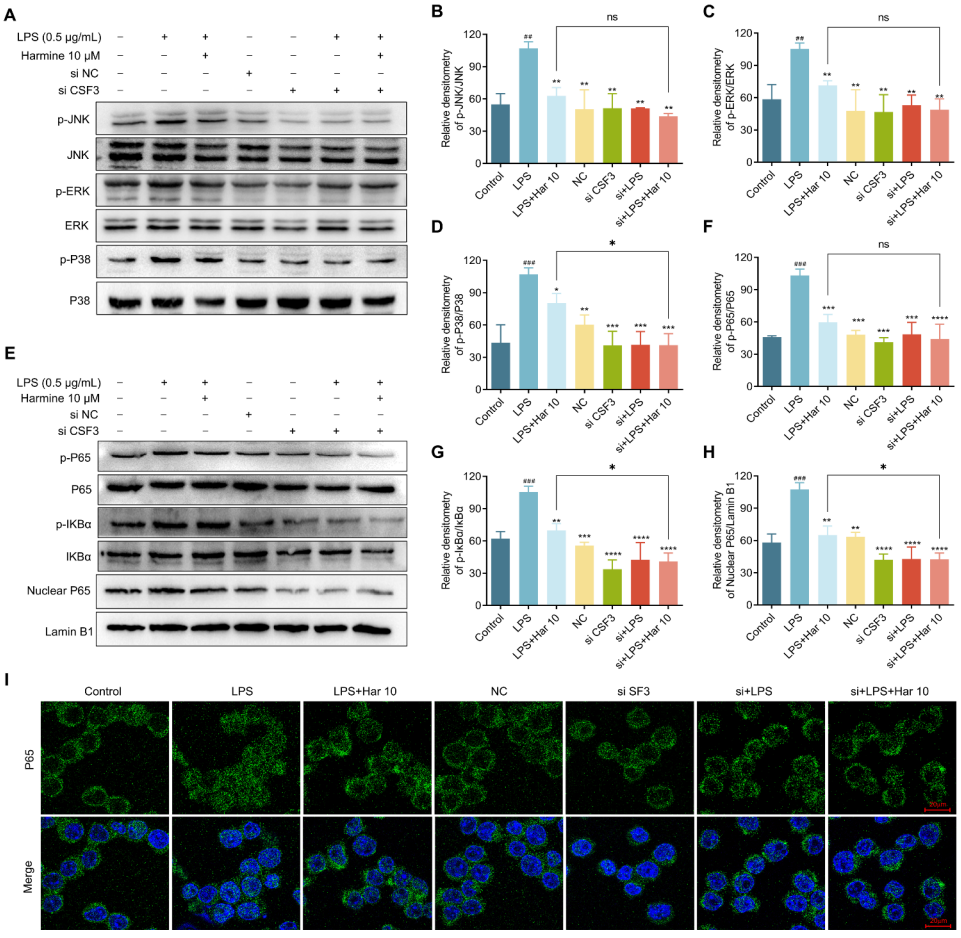

Fig. 8 Harmine blocked the activation of MAPK/NF-κB signaling pathway by inhibiting CSF3 expression. Cells was transfected with siRNA for 8 h, then pre-treated with harmine for 30 min, followed by exposure to LPS (0.5 μg/mL) for 6 h before being used in western blot and IF assays. (**A** and **E**) Western blot detected the p-JNK, JNK, p-ERK, ERK, p-P38, P38, p-IκBα, IκBα, p-P65, P65 and nuclear P65 proteins levels. β-actin or Lamin B1 was used as the loading control ($n = 3$). (**B**-**D** and **F**-**H**) Quantitative analysis of (**A**) and (**E**), respectively. (**I**) IF staining assay examined the translocation of P65 from the cytoplasm to the nucleus. Values represent as the mean ± SD of at least three independent experiments. Scale bar, 20 μm. ns, no significance; $^{*}p < 0.05$; $^{**}p < 0.01$; $^{***}p < 0.001$, $^{****}p < 0.0001$, vs. LPS group. $^{\#\#}p < 0.01$; $^{\#\#\#}p < 0.001$, vs. control group

TNF-α (Fig. 6G-I). Furthermore, GEO database analysis indicated that CSF3 is markedly overexpressed in ALI/ARDS (Fig. 6J).

The effect of harmine on CSF3 transcription and expression was further evaluated by qPCR and western blot assays in harmine-pretreated or untreated LPS-stimulated RAW264.7 cells or the lung tissue of LPS-induced ALI mice. The results suggested that LPS stimulation significantly increased CSF3 transcription and expression, while harmine pretreatment reduced LPS-enhanced CSF3 transcription and expression levels in a dose-dependent manner both in RAW264.7 cells and lung tissue of LPS-induced ALI mice (Fig. 6K-P). Taken together, these findings strongly supported that harmine provides a protective effect against LPS-indued ALI involving CSF3.

Harmine inhibits LPS-induced inflammation through CSF3-mediated MAPK/NF-κB inactivation

To verify this hypothesis, CSF3 was knocked down by siRNA, and a series of assays were re-performed in LPS-stimulated RAW264.7 cells. Since si-2 siRNA exhibited the strongest CSF3 silencing efficiency (Fig. 7A-C), it was selected for subsequent assays. Western blot results indicated that LPS stimulation did not enhance CSF3 expression in CSF3-silenced RAW264.7 cells compared to CSF3-intact cells (Fig. 7D-E). qPCR results suggested that LPS stimulation failed to induce high levels of IL-6, IL-1β, and TNF-α mRNA transcription in CSF3-silenced RAW264.7 cells as it did in CSF3-intact cells (Fig. 7F-H). Moreover, harmine exhibited a stronger inhibitory effect on IL-6, IL-1β, and TNF-α mRNA transcription in CSF3-silenced RAW264.7 cells than in CSF3-intact cells (Fig. 7F-H), suggesting a positive correlation

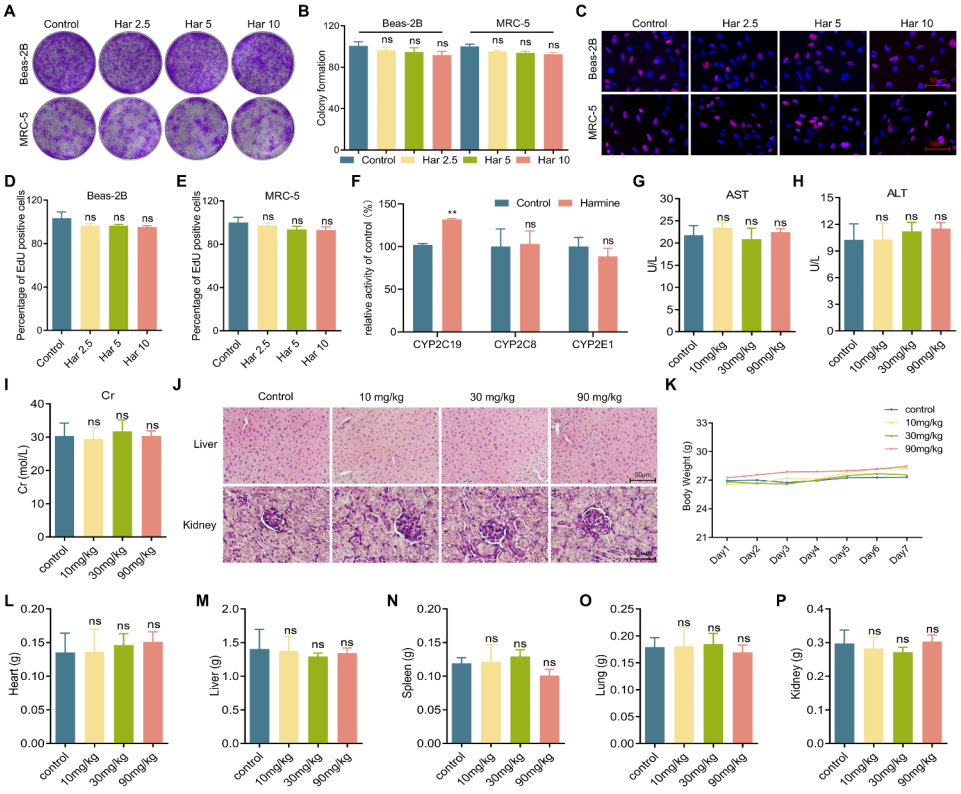

Fig. 9 Harmine exhibited high biological safety both in vitro and in vivo. (**A**) Colony formation assay of human normal lung cell Beas-2B and MRC-5 cells. Cells were co-cultured with harmine at the indicated doses for 7 days before imaging. (**B**) Quantitative analysis of (A). (**C**) EdU staining assay assessed the DNA replication rate of Beas-2B and MRC-5 cells following a 24 h exposure to harmine at the indicated doses. Scale bar, 50 μm. (**D** and **E**) Quantitative analysis of (**C**). (**F**) Effect of harmine on liver drug enzyme activity. (**G-I**) Serum levels of ALT, AST and Cr in mice. (**J**) H&E staining of liver and kidney tissue. Scale bar, 50 μm. (**K**) Daily weight changes in mice during acute toxicity experiments. (**L-P**) Weight changes of the heart, liver, spleen, lung and kidney in mice after 7 days. Mice were administrated harmine orally at the indicated doses and continue feeding for 7 days before sacrifice. Values represent as the mean ± SD of at least three independent experiments. ns, no significance; $^{**}p < 0.01$, vs. control group

between CSF3 expression levels and inflammatory cytokines mRNA transcription levels. Similarly, ELISA assay indicated that LPS stimulation failed to enhance the secretion of inflammatory factors in CSF3-silenced RAW264.7 cells compared to CSF3-intact cells (Fig. 7I-K), and harmine pretreatment resulted in lower levels of IL-6, IL-1β, and TNF-α protein in CSF3-silenced RAW264.7 cells than in CSF3-intact cells (Fig. 7I-K).

The regulatory effect of CSF3 on the MAPK/NF-κB signaling pathway was explored. LPS stimulation strongly enhanced the phosphorylation of JNK, ERK, and P38 in RAW264.7 cells, while it moderately enhanced the phosphorylation of these MAPKs in CSF3-silenced cells (Fig. 8A-D), indicating that LPS lost most of its ability to activate the MAPK signaling pathway in CSF3-silenced cells. Additionally, LPS failed to enhance the phosphorylation of P65, nucleus P65, and IκBα in CSF3-silenced RAW264.7 cells as it did in CSF3-intact cells (Fig. 8E-H). Furthermore, harmine exhibited a stronger inhibitory effect on LPS-induced NF-κB signaling pathway activation in CSF3-silenced RAW264.7 cells than in CSF3-intact RAW264.7 cells (Fig. 8E-H), which was further supported by the IF assay (Fig. 8I). In conclusion, these results suggested that harmine inhibited LPS-induced inflammation in ALI by inactivating the CSF3-mediated MAPK/NF-κB signaling pathway.

Harmine has high biological safety

The biological safety of harmine was evaluated in vitro and in vivo. Colony formation and EdU staining assays were conducted using normal human lung cells BEAS-2B and MRC-5. The results showed that harmine had almost no inhibitory effect on the proliferation and DNA replication of BEAS-2B and MRC-5 (Fig. 9A-E), demonstrating that harmine does not exhibit toxicity in normal lung cells. Consistently, results from MTT and FACS assays also indicated that harmine does not cause cytotoxicity or apoptosis in BEAS-2B and MRC-5 (Figs. S4-S5). Drug-induced liver and kidney injury and dysfunction are among the main toxic side effects of natural products [42]. Thus, the effect of harmine on liver Cytochrome P450 (CYP) was assessed, and the results demonstrated that while

harmine significantly affected CYP2C19 activity, it had minimal impact on CYP2C8 and CYP2E1 activity (Fig. 9F). Moreover, the levels of AST, ALT, Cr in the serum of harmine-treated mice were comparable to those in control mice (Fig. 9G-I). These findings demonstrated that harmine had limited adverse effect on liver and kidney function. Additionally, histological analysis indicated that harmine treatment did not cause organic lesions in the liver and kidney (Fig. 9J). Furthermore, there was no significant difference in the body weight of the mice and the organ weights of the heart, liver, spleen, lung, and kidney between control mice and harmine-treated mice (Fig. 9K-P). Overall, these results suggested that harmine has high biological safety.

Discussion

ALI, which can progress into ARDS, presents a significant clinical challenge due to its high incidence, high mortality, and lack of safe and effective treatment options [1]. The development of novel therapeutic drugs is imperative to address this unmet medical need [2]. This study aimed to investigate the therapeutic effects and molecular mechanisms of harmine against ALI. The findings demonstrated that harmine significantly inhibited LPS-induced inflammation in a dose-dependent manner by blocking CSF3-mediated MAPK/NF-κB signaling pathway activation in both LPS-induced RAW264.7 cells and ALI mice (Figs. 1, 2, 3 and 8), leading to strong protective and therapy effects against LPS-induced lung injury in ALI mice (Figs. 4 and 5). Considering its high biological safety (Fig. 9), these findings indicated that harmine could be a potential ALI therapeutic drugs for ALI.

Macrophages and neutrophils, which generate excessive proinflammatory cytokines [43], play a key role in the pathological progression of ALI [1]. Thus, reducing the recruitment and infiltration of macrophages and neutrophils is a feasible strategy for ALI therapy [44]. In this study, harmine pretreatment significantly inhibited LPS-induced infiltration of macrophages and neutrophils in lung tissues (Fig. 4F-H). Additionally, harmine pretreatment significantly suppressed the LPS-induced gene expression of adhesion molecules ICAM-1 and VCAM-1 in lung tissues (Fig. 4I), which might partly contribute to the reduction of neutrophils infiltration. Moreover, harmine restored LPS-stimulated increased permeability of the alveolar-capillary barrier (Figs. 4A-B and E and 5A and D-E), a typical characteristic of ALI [45], which might also contribute to the alleviation of immune cells infiltration and inflammatory response. Together, these findings suggested that inhibiting the infiltration of immune cells contributed to the protective effect of harmine against LPS-induced lung injury in ALI mice.

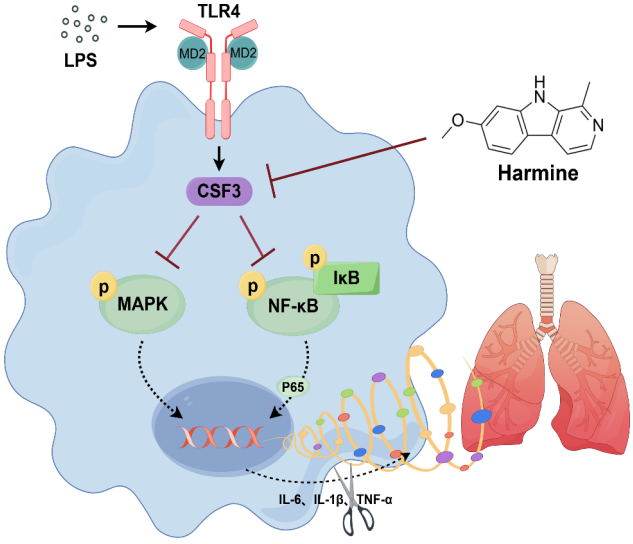

Fig. 10 Mechanism illustration of the present study. Harmine inhibited inflammation by blocking CSF3-mediated MAPK/NF-κB signaling pathway activation, thereby reducing LPS-induced inflammatory factor storm and ultimately alleviating LPS-induced ALI in mice

TLR4-MD2 has been demonstrated as a classical immune regulatory complex for downstream MAPK/NF-κB signaling pathway activation in LPS-induced ALI [46]. Surprisingly, harmine has no apparent effect on the LPS-induced enhanced binding interaction between TLR4 and MD2 (Fig. S3). In contrast, the findings indicated that harmine pretreatment significantly inhibited LPS-induced inflammatory responses by suppressing the transcription and expression of CSF3 (Fig. 6A-B and K-P), a cytokine critical to the immune response [17]. Previous studies have shown that CSF3 regulates the MAPK/NF-κB signaling pathway in non-inflammatory disease [20]. In this study, it was found that LPS failed to activate the MAPK/NF-κB signaling pathway in CSF3-silenced RAW264.7 cells as it did in CSF3-intact RAW264.7 cells (Fig. 8), resulting in significantly inhibited expression and secretion of inflammatory factors under LPS stimulation (Fig. 7F-K). A key limitation of this study is the absence of established pharmacological treatments for ALI, hindering the use of a positive control. This limitation highlights the unique potential of harmine as a groundbreaking therapy. Taken together, these findings suggested that CSF3 could serve as a novel potential target for ALI treatment, and that harmine alleviates LPS-induced inflammation by CSF3 inhibition-mediated MAPK/NF-κB signaling pathway inactivation (Fig. 10).

Conclusion

In conclusion, the findings elucidated that harmine protects against LPS-induced ALI by inhibiting the infiltration of immune cells and the CSF3-mediated inactivation of the MAPK/NF-κB signaling pathway, thereby reducing LPS-induced inflammation. This study provides important insights into the preventive and therapeutic potential of harmine for the treatment of ALI. Additionally, our cellular-level experiments and acute toxicity indicate that harmine does not cause significant adverse effects, suggesting a favorable biological safety profile. These findings supported the potential of harmine as a therapeutic agent for ALI and other inflammatory diseases.

Abbreviations

ALI	Acute lung injury
ARDS	Acute respiratory distress syndrome
CSF3	Granulocyte Colony-Stimulating Factor
NF-κB	Nuclear factor kappa B
MAPK	Mitogen-activated protein kinase
MTT	3-(4,5-dimethylthiazol-2-yl)-2,5-diphenyltetrazolium bromide
H&E	Hematoxylin-eosin
IHC	Immunohistochemical
ELISA	Enzyme-linked immunosorbent assay
IF	Immunofluorescence
qPCR	Real-time quantitative PCR
Co-IP	Co-immunoprecipitation
ICAM-1	Intercellular adhesion molecule 1
VCAM-1	Vascular cell adhesion molecule 1
ECMO	Extracorporeal membrane oxygenation
PPI	Protein-protein interaction
GEO	Gene Expression Omnibus
ALT	Alanine aminotransferase
AST	Aspartate aminotransferase
Cr	Creatinine
CYP	Cytochrome P450
SD	Standard deviation

Supplementary Information

The online version contains supplementary material available at https://doi.org/10.1186/s12931-025-03196-8.

Supplementary Material 1

Supplementary Material 2

Acknowledgements

Not applicable.

Author contributions

Y.Z. performed data curation and project administration, wrote the main manuscript text. K.C. performed project administration. Z.X. performed conceptualization and data curation. X.C., J.T., Y.H., C.C., and M. D. performed project administration and analyzed the data. G. L. and X. Z. desinged the project and wrote the main manuscript text. All authors reviewed the manuscript.

Funding

This work was supported by the Natural Science Foundation of Zhejiang Province (LY22H310004), the National Natural Science Foundation of China (82273995), the Wenzhou Basic Medical and Health Technology Project (Y20220190), We thank Scientific Research Center of Wenzhou Medical university and Wenzhou Key Laboratory of Research and Transformation of Chinese Medicine for consultation and instrument availability that supported this work. Figure 9 was drawn with Figdraw (www.ffgdraw.com).

Data availability

No datasets were generated or analysed during the current study.

Declarations

Competing interests

The authors declare no competing interests.

Ethics approval and consent to participate

Ethical approval for all animal care and experimental procedures was obtained from the Animal Policy and Welfare Committee of Wenzhou Medical University (approval number: xmsq2021-0043).

Author details

[1]School of Pharmaceutical Sciences, Wenzhou Medical University, Wenzhou 325035, Zhejiang, China

Received: 18 December 2024 / Accepted: 18 March 2025
Published online: 28 March 2025

References

1. Scozzi D, Liao F, Krupnick AS, Kreisel D, Gelman AE. The role of neutrophil extracellular traps in acute lung injury. Front Immunol. 2022;13953195.
2. Lin P, Gao R, Fang Z, Yang W, Tang Z, Wang Q, Wu Y, Fang J, Yu W. Precise nanodrug delivery systems with cell-specific targeting for ALI/ARDS treatment. Int J Pharm. 2023;644123321.
3. Hu Q, Zhang S, Yang Y, Yao JQ, Tang WF, Lyon CJ, Hu TY, Wan MH. Extracellular vesicles in the pathogenesis and treatment of acute lung injury. Mil Med Res. 2022;9(1):61.
4. He YQ, Zhou CC, Yu LY, Wang L, Deng JL, Tao YL, Zhang F, Chen WS. Natural product derived phytochemicals in managing acute lung injury by multiple mechanisms. Pharmacol Res. 2021;163105224.
5. Zambon M, Vincent JL. Mortality rates for patients with acute lung injury/ards have decreased over time. Chest. 2008;133(5):1120–7.
6. Zhou X, Liao Y. Gut-Lung crosstalk in Sepsis-Induced acute lung injury. Front Microbiol. 2021;12779620.
7. Liu C, Xiao K, Xie L. Advances in the regulation of macrophage polarization by mesenchymal stem cells and implications for ALI/ARDS treatment. Front Immunol. 2022;13928134.
8. Wang Z, Yu T, Hou Y, Zhou W, Ding Y, Nie H. Mesenchymal stem cell therapy for ALI/ARDS: therapeutic potential and challenges. Curr Pharm Des. 2022;28(27):2234–40.
9. Combes A, Peek GJ, Hajage D, Hardy P, Abrams D, Schmidt M, Dechartres A, Elbourne D. ECMO for severe ARDS: systematic review and individual patient data meta-analysis. Intensive Care Med. 2020;46(11):2048–57.
10. Shen B, Zhang H, Zhu Z, Ling Z, Zeng F, Wang Y, Wang J. Baicalin relieves LPS-Induced lung inflammation via the NF-kappaB and MAPK pathways. Molecules. 2023;28(4).
11. Liao J, Yang J, Li X, Hu C, Zhu W, Zhou Y, Zou Y, Guo M, Chen Z, Li X, Dai J, Xu Y, Zheng Z, Chen P, Cho WJ, Liang G, Tang Q. Discovery of the Diphenyl 6-Oxo-1,6-dihydropyridazine-3-carboxylate/carboxamide analogue J27 for the treatment of acute lung injury and sepsis by targeting JNK2 and inhibiting the JNK2-NF-kappaB/MAPK pathway. J Med Chem. 2023;66(17):12304–23.
12. Li Z, Pan H, Yang J, Chen D, Wang Y, Zhang H, Cheng Y. Xuanfei Baidu formula alleviates impaired mitochondrial dynamics and activated NLRP3 inflammasome by repressing NF-kappaB and MAPK pathways in LPS-induced ALI and inflammation models. Phytomedicine. 2023;108154545.
13. Hong H, Lou S, Zheng F, Gao H, Wang N, Tian S, Huang G, Zhao H. Hydnocarpin D attenuates lipopolysaccharide-induced acute lung injury via MAPK/NF-kappaB and Keap1/Nrf2/HO-1 pathway. Phytomedicine. 2022;101154143.
14. Zhou M, Meng L, He Q, Ren C, Li C. Valsartan attenuates LPS-induced ALI by modulating NF-kappaB and MAPK pathways. Front Pharmacol. 2024;151321095.
15. Son ES, Ko UW, Jeong HY, Park SY, Lee YE, Park JW, Jeong SH, Kim SH, Kyung SY. miRNA-6515-5p regulates particulate matter-induced inflammatory responses by targeting CSF3 in human bronchial epithelial cells. Toxicol Vitro. 2022;84105428.

16. Ouyang S, Liu C, Xiao J, Chen X, Lui AC, Li X. Targeting IL-17A/glucocorticoid synergy to CSF3 expression in neutrophilic airway diseases. JCI Insight. 2020;5(3).
17. McGrath JJC, Vanderstocken G, Dvorkin-Gheva A, Cass SP, Afkhami S, Fantauzzi MF, Thayaparan D, Reihani A, Wang P, Beaulieu A, Shen P, Morissette M, Jimenez-Saiz R, Revill SD, Tabuchi A, Zabini D, Lee WL, Richards CD, Miller MS, Ask K, Kuebler WM, Simpson JA, Stampfli MR. Cigarette smoke augments CSF3 expression in neutrophils to compromise alveolar-capillary barrier function during influenza infection. Eur Respir J. 2022;60(2).
18. Petrina M, Martin J, Basta S. Granulocyte macrophage colony-stimulating factor has come of age: from a vaccine adjuvant to antiviral immunotherapy. Cytokine Growth Factor Rev. 2021;59101–110.
19. Liu D, Zhang Y, Zhen L, Xu R, Ji Z, Ye Z. Activation of the NFkappaB signaling pathway in IL6 + CSF3 + vascular endothelial cells promotes the formation of keloids. Front Bioeng Biotechnol. 2022;10917726.
20. Marino VJ, Roguin LP. The granulocyte colony stimulating factor (G-CSF) activates Jak/STAT and MAPK pathways in a trophoblastic cell line. J Cell Biochem. 2008;103(5):1512–23.
21. Su J, Zhou H, Tao Y, Guo J, Guo Z, Zhang S, Zhang Y, Huang Y, Tang Y, Dong Q, Hu R. G-CSF protects human brain vascular endothelial cells injury induced by high glucose, free fatty acids and hypoxia through MAPK and Akt signaling. PLoS ONE. 2015;10(4):e0120707.
22. Li H, Linjuan L, Wang Y. G-CSF improves CUMS-induced depressive behaviors through downregulating Ras/ERK/MAPK signaling pathway. Biochem Biophys Res Commun. 2016;479(4):827–32.
23. Zhao X, Kawano SI, Masuda J, Murakami H. G-CSF-dependent neutrophil differentiation requires downregulation of MAPK activities through the Gab2 signaling pathway. Cell Biol Int. 2020;44(9):1919–33.
24. Guo Y, Liu S, Zhang X, Wang L, Gao J, Han A, Hao A. G-CSF promotes autophagy and reduces neural tissue damage after spinal cord injury in mice. Lab Invest. 2015;95(12):1439–49.
25. Guan ZF, Tao YH, Zhang XM, Guo QL, Liu YC, Zhang Y, Wang YM, Ji G, Wu GF, Wang NN, Yang H, Yu ZY, Guo JC, Zhou HG. G-CSF and cognitive dysfunction in elderly diabetic mice with cerebral small vessel disease: preventive intervention effects and underlying mechanisms. CNS Neurosci Ther. 2017;23(6):462–74.
26. Wiedermann FJ, Mayr AJ, Hobisch-Hagen P, Fuchs D, Schobersberger W. Association of endogenous G-CSF with anti-inflammatory mediators in patients with acute respiratory distress syndrome. J Interferon Cytokine Res. 2003;23(12):729–36.
27. Hierholzer C, Kelly E, Lyons V, Roedling E, Davies P, Billiar TR, Tweardy DJ. G-CSF instillation into rat lungs mediates neutrophil recruitment, pulmonary edema, and hypoxia. J Leukoc Biol. 1998;63(2):169–74.
28. Wiedermann FJ, Mayr AJ, Kaneider NC, Fuchs D, Mutz NJ, Schobersberger W. Alveolar granulocyte colony-stimulating factor and alpha-chemokines in relation to serum levels, pulmonary neutrophilia, and severity of lung injury in ARDS. Chest. 2004;125(1):212–9.
29. Jin SJ, Song Y, Park HS, Park KW, Lee S, Kang H. Harmine Inhibits Multiple TLR-Induced Inflammatory Expression through Modulation of NF-kappaB p65, JNK, and STAT1. Life (Basel). 2022;12(12).
30. Fan R, Wang S, Wu Y, Feng Y, Gao M, Cao Y, Ma X, Xie S, Wang C, Gao L, Wang Y, Dai F. Activation of Endoplasmic reticulum stress by Harmine suppresses the growth of esophageal squamous cell carcinoma. Phytother Res. 2023;37(10):4655–73.
31. Shi Y, Chen X, Shu J, Liu Y, Zhang Y, Lv Q, Wang J, Deng X, Liu H. and Qiu J. Harmine, an inhibitor of the type III secretion system of Salmonella enterica serovar typhimurium. Front Cell Infect Microbiol. 2022;12967149.
32. Ruan W, Ji X, Qin Y, Zhang X, Wan X, Zhu C, Lv C, Hu C, Zhou J, Lu L, Guo X. Harmine alleviated Sepsis-Induced cardiac dysfunction by modulating macrophage polarization via the STAT/MAPK/NF-kappaB pathway. Front Cell Dev Biol. 2021;9792257.
33. Wang L, Wang Q, Wang W, Ge G, Xu N, Zheng D, Jiang S, Zhao G, Xu Y, Wang Y, Zhu R, Geng D. Harmine alleviates titanium Particle-Induced inflammatory bone destruction by Immunomodulatory effect on the macrophage polarization and subsequent osteogenic differentiation. Front Immunol. 2021;12657687.
34. Niu X, Yao Q, Li W, Zang L, Li W, Zhao J, Liu F, Zhi W. Harmine mitigates LPS-induced acute kidney injury through Inhibition of the TLR4-NF-kappaB/NLRP3 inflammasome signalling pathway in mice. Eur J Pharmacol. 2019;849160–169.
35. Chen J, Jin X, Shen Z, Mei Y, Zhu J, Zhang X, Liang G, Zheng X. H(2)O(2) enhances the anticancer activity of TMPyP4 by ROS-mediated mitochondrial dysfunction and DNA damage. Med Oncol. 2021;38(6):59.
36. Jin XX, Mei YN, Shen Z, Zhu JF, Xing SH, Yang HM, Liang G, Zheng XH. A chalcone-syringaldehyde hybrid inhibits triple-negative breast cancer cell proliferation and migration by inhibiting CKAP2-mediated FAK and STAT3 phosphorylation. Phytomedicine. 2022;101154087.
37. Zhang YL, Zhang WX, Yan JQ, Tang YL, Jia WJ, Xu ZW, Xu MJ, Chattipakorn N, Wang Y, Feng JP, Liu ZG, Liang G. Chalcone derivatives ameliorate lipopolysaccharide-induced acute lung injury and inflammation by targeting MD2. Acta Pharmacol Sin. 2022;43(1):76–85.
38. Fang B, Lai Y, Yan H, Ma Y, Ni Z, Zhu Q, Zhang J, Ye Y, Wang M, Wang P, Wang Y, Zhang S, Hui M, Wang D, Zhao Y, Li X, Wang K, Liu Z. Corrigendum to Design, synthesis, and biological evaluation of 1,6-naphthyridine-2-one derivatives as novel FGFR4 inhibitors for the treatment of colorectal cancer [Eur. J. Med. Chem. 259 (2023) 115703/5]. Eur J Med Chem. 2024;268116230.
39. Dilxat T, Shi Q, Chen X, Liu X. Garlic oil supplementation blocks inflammatory pyroptosis-related acute lung injury by suppressing the NF-kappaB/NLRP3 signaling pathway via H(2)S generation. Aging. 2024;16(7):6521–36.
40. Wang Y, Wang X, Li Y, Xue Z, Shao R, Li L, Zhu Y, Zhang H, Yang J. Xuanfei Baidu Decoction reduces acute lung injury by regulating infiltration of neutrophils and macrophages via PD-1/IL17A pathway. Pharmacol Res. 2022;176106083.
41. Li G, Jiang X, Liang X, Hou Y, Zang J, Zhu B, Jia C, Niu K, Liu X, Xu X, Jiang R, Wang B. BAP31 regulates the expression of ICAM-1/VCAM-1 via MyD88/NF-kappaB pathway in acute lung injury mice model. Life Sci. 2023;313121310.
42. Sun YK, Zhang YF, Xie L, Rong F, Zhu XY, Xie J, Zhou H, Xu T. Progress in the treatment of drug-induced liver injury with natural products. Pharmacol Res. 2022;183106361.
43. Saguil A, Fargo MV. Acute respiratory distress syndrome: diagnosis and management. Am Fam Physician. 2020;101(12):730–8.
44. Zhu W, Luo W, Han J, Zhang Q, Ji L, Samorodov AV, Pavlov VN, Zhuang Z, Yang D, Yin L, Huang L, Liang G, Huh JY, Wang Y. Schisandrin B protects against LPS-induced inflammatory lung injury by targeting MyD88. Phytomedicine. 2023;108154489.
45. Kryvenko V, Vadasz I. Alveolar-capillary endocytosis and trafficking in acute lung injury and acute respiratory distress syndrome. Front Immunol. 2024;151360370.
46. Yang L, Luo W, Zhang Q, Hong S, Wang Y, Samorodov AV, Chattipakorn N, Pavlov VN, Liang G. Cardamonin inhibits LPS-induced inflammatory responses and prevents acute lung injury by targeting myeloid differentiation factor 2. Phytomedicine. 2021;93153785.

Publisher's note